Mechanics & Industry **21**, 620 (2020)

https://doi.org/10.1051/meca/2020094

Mechanics & Industry

Available online at:
www.mechanics-industry.org

REGULAR ARTICLE

Mode and regime identification for a static NACA0012 airfoil at transitional Reynolds numbers

Allison Poels, Xavier Collin, Azemi Benaissa*, and Dominique Poirel

Department of Mechanical and Aerospace Engineering Royal Military College of Canada Kingston, Ontario K7K 7B4, Canada

Received: 21 February 2020 / Accepted: 25 November 2020

Abstract. This work examines the flow structure modes in the boundary layer and in the wake of a NACA0012 airfoil in static conditions at transitional chord-based Reynolds numbers (Re_c), for small angles of attack (α). A laminar mode, with a laminar separation of the boundary layer and laminar Kármán streets in the wake, was first observed for $Re_c < 61400$ and $\alpha = 0°$. For $77\,000 < Re_c < 118600$, which corresponds to a regime between laminar and transitional mode called subcritical mode, the boundary layer exhibited a long separation bubble reattached close to the trailing edge, and the wake showed a turbulent Kármán street. Finally, for higher Re_c and α, a critical transition mode consisted of a long bubble followed by a turbulent separation, and a less structured vortex street in the wake of the airfoil.

Keywords: Laminar separation, transitional Reynolds Number, Wake of a NACA0012 airfoil.

1 Introduction

Research in low Reynolds number flows is getting increasing attention due to the growing market of Unmaned Aerial Vehicles (UAVs) or Drones. The range of Reynolds numbers considered corresponds to small aerial vehicles or vehicles flying at high altitudes, they are more and more frequently used in civilian and military applications. The drones are becoming part of daily operations for many industries. Their design and use have generated an impressive number of companies of different sizes. This industry will continue to grow and generate among others, research in an area of aeronautic that was not explored for this type of application. Flexible structures used to build these vehicles, are sensitive to flow perturbations. The interaction between the flow and the structure can lead to self-sustained oscillations such as limit cycle oscillations (LCO), such oscillations could be damageable. But they are also considered for research on new sustainable energy. Underwater energy harvesters have been the subject of promising studies (Kinsey et al. [1]).

The aerodynamics in the case of an airfoil at low Reynolds numbers is very specific and different when compared to the high Reynolds number case. Below $Re_c = 5 \times 10^5$, which corresponds to the boundary layer transition threshold, the flow is very unsteady; a laminar separation bubble (LSB) appears and aerodynamic performances decrease rapidly. The LSB is subject to instability phenomenon resulting from the fluid motion inside the bubble and the free flow on top of the bubble. Gaster [2] investigated the parameters that characterise short and long bubbles. He used two mean flow parameters to control bursting: pressure-gradient parameter and the Reynolds number based on the displacement thickness, both calculated at the separation location. Marxen and Henningson [3] have considered the bursting of the LSB using numerical simulation. They identified two types of bursting, one is observed after turbulent reattachment. It happens during the start-up of the disturbance. The second happens during switch-off of the disturbance, in this case, transition does not lead to reattachment. The interest in flow structure interaction has also considered the wake and the separated boundary layer over a cylinder [4,5]. For instance, Williamson [5] did a comprehensive review of the subject from an aeroelastic point of view since the flow unsteadiness can induce structural vibrations or even oscillatory motion that can lead to an active interaction mechanism between the structure and the flow. For 2D airfoils immersed in a flow at low Reynolds number, most of the studies have focused on the aerodynamic performance analysis, bubble visualization and characterization, surveying 2D shear layer instability. For instance, Carmichael [6] and Lissaman [7] have documented these fields. The wake structure is also very specific and can induce forces on the airfoil and modify its performance.

* e-mail: benaissa-a@rmc.ca

Specifically, the shedding of the LSB and/or Kármán vortex streets could be, either apparent or submerged in a turbulent flow. They affect the air flow around the structure.

In the effort of a better understanding of the flow behavior over a lifting surface, more recently researchers have considered the flow around a NACA0012 airfoil using Direct Numerical Simulations (DNS) [8] and Large Eddy Simulations (LES) [9]. They have determined the separation and reattachement locations at an angle of attack of 5°. There is a need for experimental data to validate such interesting findings and future simulations.

In this study, we investigated the boundary layer and the wake in the same experimental setup. We considered the flow around a static NACA0012 airfoil in the range of Reynolds numbers over which low angle self-sustained oscillations have been observed in the case of an elastically mounted wing [10,11]. These oscillations are self-sustained and thus considered as limit cycle oscillations (LCO). They have low amplitude and frequency. LCO have been observed for a NACA0012 airfoil at a chord Reynolds numbers from $50000 < \mathrm{Re}_c < 130000$. This self-sustained oscillatory motion of the airfoil has been well-documented experimentally [10,12,13]. The pitching frequencies were low, close to the quasi-steady limit, however there was no evidence *a priori* that the flow over the airfoil in the static case would be similar to the flow over the pitching airfoil. The angle of attack was varied from 0° to 6°, range of angles reached during the low angle LCO. The first objective was to document the flow over the airfoil and in the near wake to understand the transient regime for this airfoil evolution with the angle of attack. This will also help identify any change in the aerodynamics within the range of Reynolds numbers studied. The second objective was to document the flow in terms of structure components with a possible signature of the boundary activity (LSB) in the wake. These results can be compared to the oscillating airfoil data.

2 Experimental methods

2.1 Experimental setup

The experiments were performed in a closed-loop low speed wind tunnel as shown in Figure 1. The operating velocity ranges from 5 m/s to 50 m/s and is controlled via a variable speed fan. The corresponding Re_c ranged from 5×10^4 to 5.5×10^5. The test section dimensions are 0.76m by 1.08m. The 2D free stream velocity vectors at the mid-test section for the highest speed shows a homogeneous and steady flow. The measured turbulence intensity at the highest experimental speed is about 0.15%.

The free-stream velocity was measured with a pitot-static tube, located upstream of the test section, connected to a pressure transducer. The average value of the pressure transducer response was obtained via a voltmeter. The flow temperature was also measured with a thermocouple placed at the exit of the test section. Since the tests were performed at low Re_c numbers, special care was taken in order to maintain the same conditions and parameters for all tests.

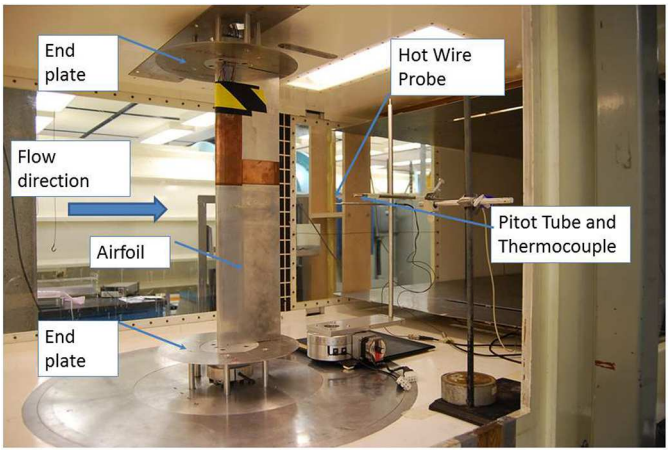

Fig. 1. Experimental Rig for the NACA0012 airfoil used for the wake measurements.

The tests consisted of two setups, one for the boundary layer oil flow visualization and one for hot wire measurements. The first airfoil was set horizontally the second was held vertically. The horizontal and vertical NACA0012 airfoils have a chord (C) of 12 cm and 15.6 cm, respectively. They had the same aspect ratio of 3.4. Their surface was smooth. The horizontal airfoil was mantained with two supports in the center of the wind tunnel test section. Its top surface was coated with fluorescent paraffin oil for flow visualization. The exposure time for the oil-flow visualization tests was set to 30–45 minutes to ensure a steady state spread of the oil. The air flow was then stopped and a CCD Casio Exilim camera equipped with pre-set night filters (UV detection) was installed, along with an ultra-violet light, to get the photographs. Although the surface oil visualization technique may be inadequate if the surface roughness is modified by the presence of a viscous liquid layer, which could influence the boundary layer, it appears that when the technique is used at Reynolds numbers higher than 3×10^4 (McGranahan and Selig [14], no major influence of the oil layer should be detected). The vertical airfoil was assigned to wake measurements. In each case, end plates were installed on both tips to minimize 3D flow effects. Indeed, oil-flow visualizations demonstrated quasi-2D flow on most of the wing span length, especially for the separation point. For reattachment, an average line was drawn to determine the separation position. It resulted in a maximum of 2.5% C error in its location.

The flow velocity and temperature were controlled via a pitot tube and a thermocouple placed in the uniform flow. The unsteady flow measurement behind the vertically fixed airfoil was performed with an X-wire probe to capture the velocity components in the streamwise and transversal directions. The X-wire probe had an opening angle of 90°. Both wires were 0.8 mm long and were 0.75 mm apart, resulting in a spatial resolution of about 1 m. They were made of tungsten wire of 5 μm diameter. A single wire probe was also used in the airfoil wake

its lenght was 0.7 mm long. A DANTEC 56C17 CTA bridge coupled to a 56N20 signal conditioning unit were used. The signals were acquired with a 12 bit data acquisition board over a minute period at 1 KHz sampling rate (60000 data points) to achieve a statistic convergence. They were filtered with a 1 KHz low pass filter. They were also amplified by a gain of 50 or 100 depending on the airflow speed.

2.2 Error analysis

The manometer and thermometer of the laboratory weather station indicates an error on the measured atmospheric pressure and ambient temperature of 0.50 Pa and 0.1 K, respectively. From the ideal gas law, the calculated error on the air density was 0.001 kg/m^3, it resulted in an error on the free stream velocity of 0.7 m/s. The error on the angle of attack positionning was in the range of $\pm$ 0.2 degrees. The signal analyis was performed with an FFT algorithm with a window of 256 data points that led to a frequency resolution on the power spectra of Δf = 0.0153 Hz. Separation positions are drawn from visualisation pictures and are estimated with 1% X/C error, while for reattachement location, error was higher (2.5% X/C). The reason of this difference being the smaller variation of the separation in the transversal direction.

3 Results

Poirel et al. [10] reported the results of the LCO of the rigid airfoil, but elastically mounted in pitch. Results were obtained for three different structural pitch stiffness coefficients, K_θ. Amplitude and reduced frequency ($k = fC/2U$, where f was the pitching frequency) were presented as a function of air speed U. They showed change in the pitching angle evolution resulting from the change in the flow characteristics over the airfoil. A first regime (FR) extends to about $\mathrm{Re}_c = 9.2 \times 10^4$. It is characterized by a relatively constant pitching angle amplitude. This amplitude depends on the mechanical stiffness imposed by the torsion springs. In this regime, the pitching frequency can be predicted with thin-airfoil theory aerodynamic. The second regime (SR), obtained for higher Reynolds numbers, is characterized by a dominating aerodynamic stiffness that increases with increasing Reynolds number. In this range, the amplitude of oscillation becomes independent of the mechanical stiffness; the airfoil oscillating motion becomes driven by aerodynamic forces. Consequently, the reduced frequency (k) exhibits constant behaviour with a small effect of the mechanical stiffness.

3.1 Boundary layer flow visualization

The boundary layer on a NACA0012 airfoil in LCO conditions has already been investigated using hot film sensors (Rudmin et al. [15,16]). In the current study, we further investigate the boundary layer aspect in the static case through oil-flow visualizations. The purpose is to understand better the flow regime at different Reynolds numbers and angles of attack. It is recognized that at transitional Reynolds numbers, the boundary layer can be very sensitive to boundary conditions. The level of turbulence in the free stream flow has a significant effect on the flow organization at the airfoil surface when turbulence intensity is below 0.45% (see Lee et al. [17]). The surface roughness is also a parameter that needs to be considered when comparing data from different experiments. These parameters can determine the occurrence of separation and influence its position.

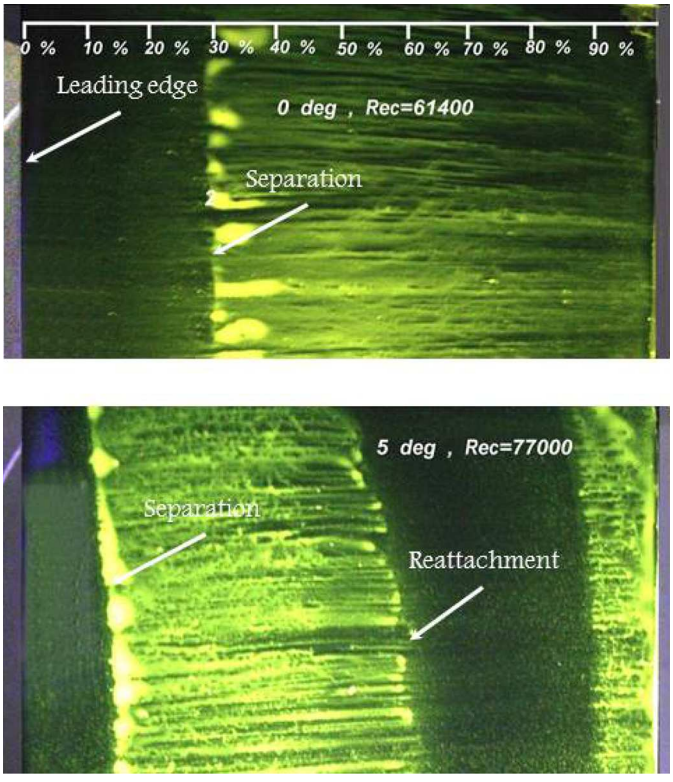

Fig. 2. Oil flow visualization of the boundary layer at $\alpha = 0°$, for $\mathrm{Re}_c = 61400$ and $\alpha = 5°$ for $\mathrm{Re}_c = 77000$.

In Figure 2, we show a sample of surface oil visualisation from which the separation and reattachment positions were found. In comparison, for the zero angle of attack case, the separation point was shown to be between 1C and 0.65C from the leading edge for a cantilever NACA0012 wing [17], in their case turbulence intensity was 0.2%. Oil-flow visualization images were also used in their case. Their wing had an aspect ratio of 5. No end plate was used in this experiment. These differences explain the disagreements in separation location between the two sets of results. Moreover, the sensitivity of the separation point to change of angle of attack is high at these small angles.

For Reynolds numbers between 5×10^4 and 13×10^4, the boundary layer is either laminar from the leading edge with a laminar separation around the mid-chord, or laminar with a laminar separation and reattachment around the trailing edge, thus forming a long LSB. These two scenarios could be present during LCO. In Figure 2,

the two scenarios are represented by surface oil visualization photographs. In the first case, for $Re_c = 61\,400$, boundary layer separation occurs at $X/C = 30\%$ for zero angle of attack. The second case is for $Re_c = 77\,000$ and an incidence angle of 5 degrees. Separation occurs at about $X/C = 10\%$ and reattachment is obtained at about $X/C = 65$ % from the leading edge. The location of the separation for increasing angle of attack from zero to five degrees for different Reynolds numbers will be discussed in the next section.

3.2 Laminar separation position

From the visualization experiments at $\alpha = 0°$ the separation point stays quasi constant at around $X/C = 30\%$ in the entire range of Reynolds numbers. For $Re_c > 1\,00\,000$, and When the airfoil is at small angles of attack (between 1 and 5 degrees), it moves downstream to around $X/C = 45\%$. The separation point moves slightly towards the trailing edge when Re_c increases. For a fixed Reynolds number, when the angle of attack increases, the separation point moves towards the leading edge. Some of these observations are plotted in Figure 3. The recent DNS results ([8]) agree with ours at 5°. While the LES of [9] does not predict reattachement at 5°. Their separation falls on Huang and lin's [18] line.

3.3 Turbulent reattachment point and size of the bubble.

It was observed that after the transition of the free shear layer, the separated flow reattached to the airfoil. The reattachment point tends to move towards the leading edge when the angle of attack or Reynolds number increases, except for $\alpha \leq 4$ degrees, where its position tends to stay the same. Thus, the size of the laminar separation bubble decreases when α or Re_c increases. However, it tends to stagnate for angles of attack between 4 and 5 degrees.

At a zero angle, we observed a laminar separation for $52\,000 < Re_c < 77\,000$ and a long laminar separation bubble for $77\,000 < Re_c < 1\,18\,600$. For Reynolds numbers above 118600, the separation point moves towards the trailing edge, to about $X/C = 50\%$. The long bubble on the suction side shortens and it is followed by a well-established turbulent boundary layer. The establishment of a turbulent boundary layer after reattachment contributes to the change in the aerodynamic moments. This was not visualized by previous studies (Huang and Lee [19], Huang and Lin [18]).

The separation points obtained through oil-flow visualizations were compared to those measured with hot-film sensors for similar Reynolds numbers and angles of attack (Rudmin et al. [16]). The separation positions found with the oil-flow visualization technique are systematically closer to the leading edge than those obtained with hot film sensors. This disagreement is attributed to the differences in the boundary conditions between the two experiments, particularly the difference in the surface state (oil and hot film sensors). The phenomena observed on both airfoils are similar, with a slight difference in the positions of the separation and reattachment with an average difference of ± 3% X/C.

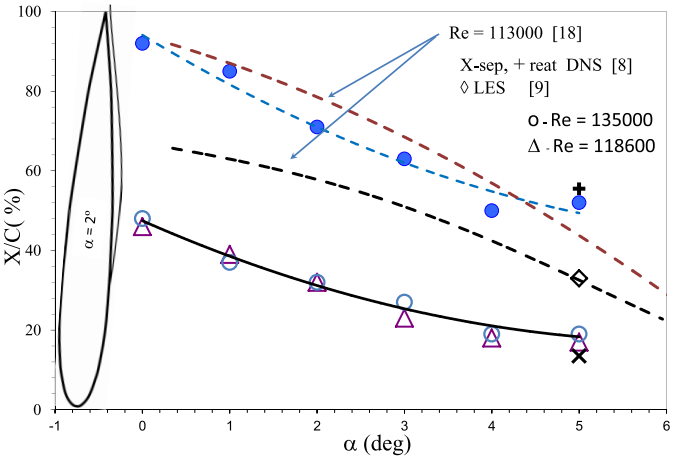

Fig. 3. Laminar separation position function of the incidence angle. Open symbols are separation and closed symbols are for reattachement. The airfoil scketch shows an example with a separation line with no reattachement (Re = 135000).

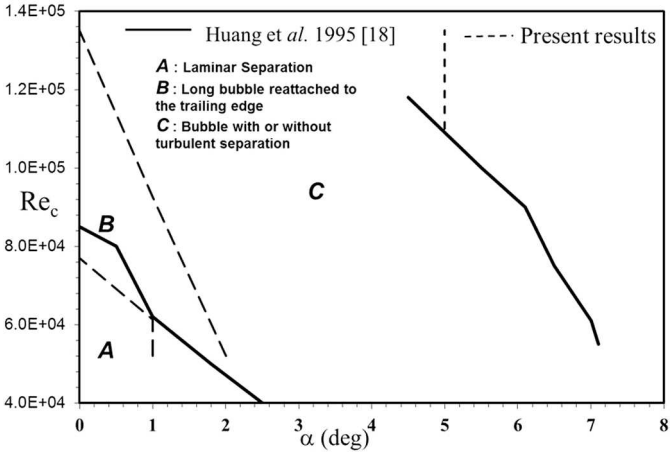

Fig. 4. Laminar separation position function of the incidence angle, for different Reynolds numbers.

3.4 Boundary layer flow regimes

For lower and similar Reynolds numbers, Huang and Lin [18] used oil-surface visualization and observed three different regimes. A comparison between their results and ours is provided in Figure 4. Our mapping of the different regimes does not match exactly their results. The region of laminar separation (A) is slightly smaller in our experiments. The area B, which was not identified in Huang and Lin's data because of the shorter cord length, corresponds in our experiments to a long bubble attached to the trailing edge, with no turbulent boundary layer. The region named C refers to the long separation bubble with a turbulent reattachment followed by a well-established turbulent boundary layer, with or without a turbulent separation. This area is wider at higher Re_c in our experiments than in Huang and Lin's study, who mentioned

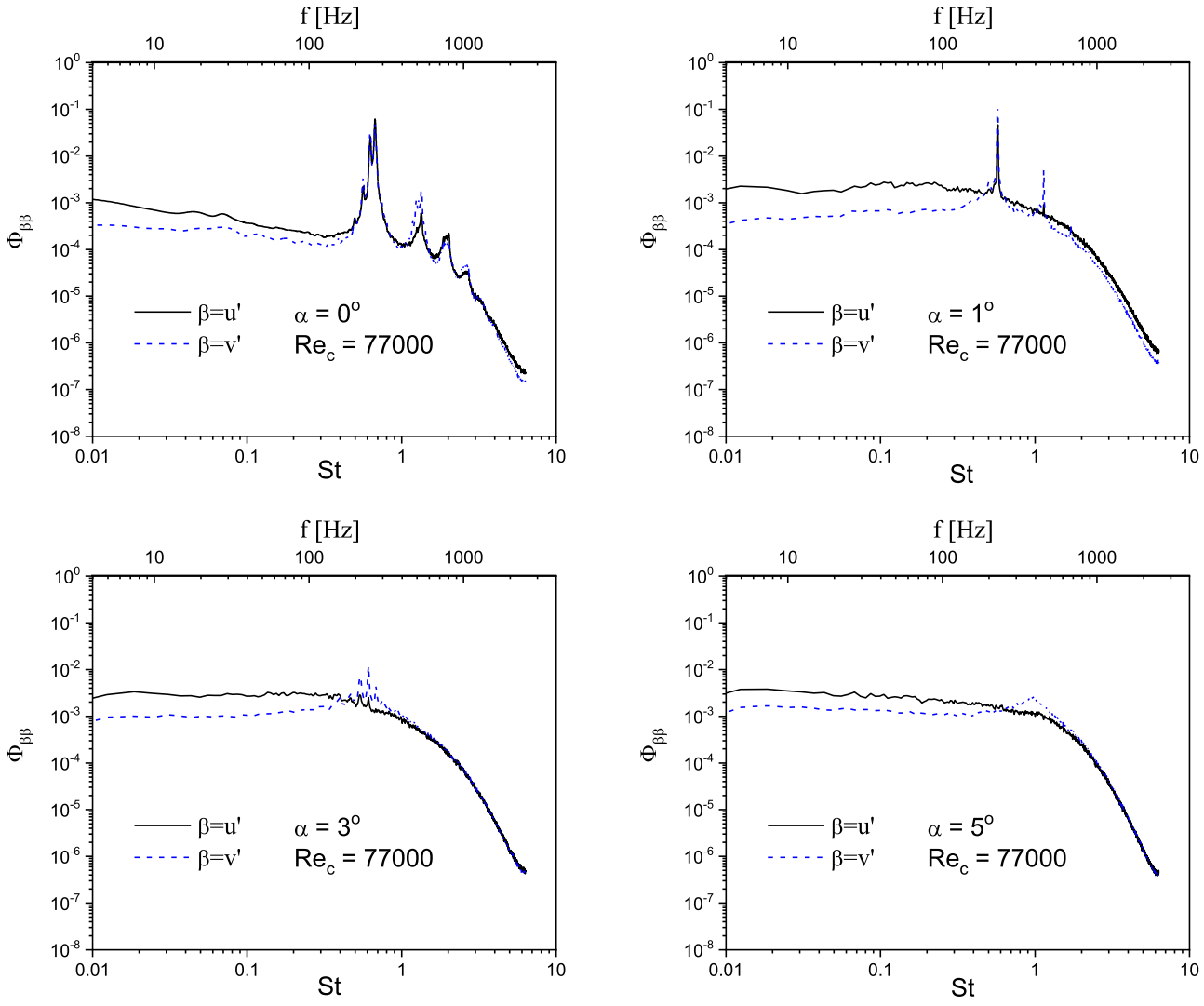

Fig. 5. Spectra of the velocity fluctuations for Re_c= 77000, at different incidence angles.

only the presence of a bubble. As previously introduced, there are experimental reasons likely to explain some of the differences between the results of the two studies. In Huang and Lin's rig, the airfoil was cantilevered without an end plate. It was placed close to the wind tunnel wall, whereas our airfoil was placed at the center of the wind tunnel with two end plates. The visualization techniques were also different and turbulence intensity in the Huang and Lin [18] study was 0.2%, higher than ours.

3.5 Near wake velocity field exploration

In this section, we present the near wake results in order to complement the view of the flow around the airfoil. Many authors have shown that a NACA0012's wake presented vortex shedding for fixed angles of attack and at small Re_c [17,18,20]. All these authors have measured the velocity fluctuations in the wake and captured the signature of the vortex shedding. They have documented the wake structure.

3.5.1 Spectral analysis of the wake velocity field

To capture the velocity fluctuations variation, the probe was positioned at X/C similar to Jung et al's work [20]. These authors concluded that Kármán streets signatures could be detected in the very near wake from $0.1C$ after the trailing edge. They also noticed that before $0.1C$, the results were distorted by the flow reversal. Furthermore, they observed similar results for frequency analyses performed at $0.1C$ and $1C$ aft of the trailing edge. We positioned the X-wire at $0.125C$ aft of the trailing edge in the wake of the airfoil, as close as possible to the airfoil in order to be sensitive to the LSB cycle and to detect vortex shedding in the wake.

A large peak is observed in the spectra at $\alpha = 0°$. It corresponds to the vortex shedding frequency. For the highest incidence angle $\alpha = 5°$ (Fig. 5), the dominant peak is not visible; this position corresponds to the maximum amplitude reached during the LCO pitching cycle. The probe position seems to be inadequate to detect the Kármán vortices. However, the spectra display a clear fully turbulent

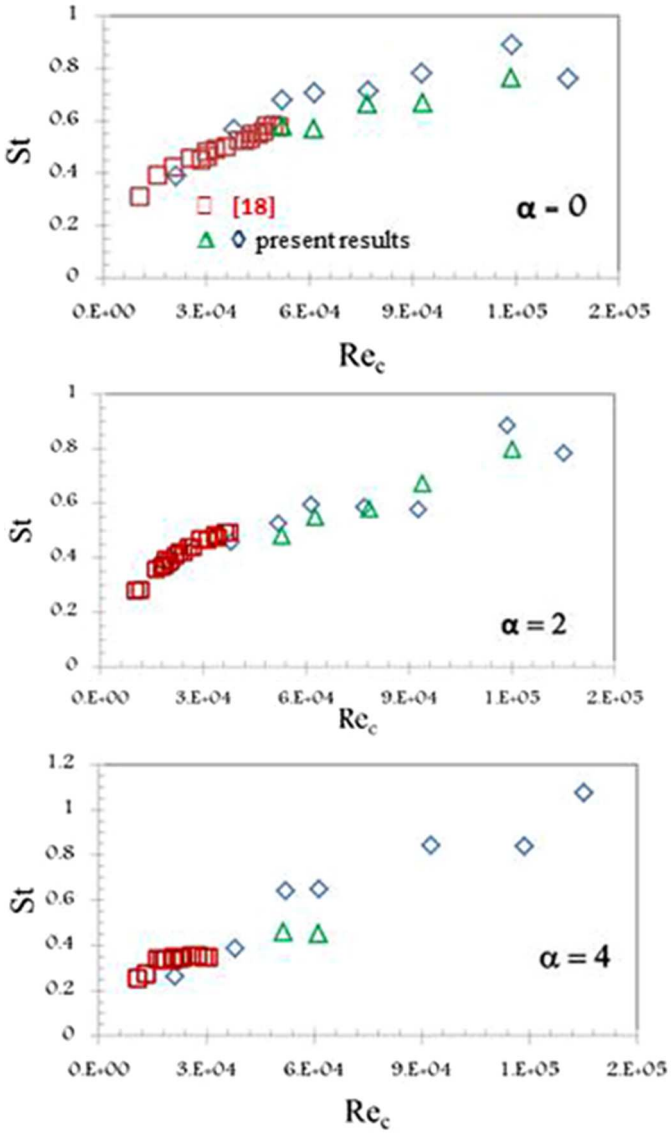

Fig. 6. Strouhal number of the main frequency peak in the wake as a function of Reynolds number.

spectrum in the C area of Figure 4. This also indicates that transition has occured.

3.5.2 Flow regime in the wake

In order to investigate better the wake and find the vortex sheeding frequencies for all angles, a single hot wire was placed $0.125C$ after the trailing edge but moved laterally to different positions for each angle to capture the wake activity and Kármán vortices signature. The spectra showed that the Kármán streets exist for large angles of attack. Over the entire range of Reynolds numbers corresponding to the occurrence of LCO, the shedding frequency and the corresponding Strouhal number increased significantly. Our results are in very good agreement with Huang and Lin's results as shown in Figure 6, for different angles of attack. The observation of our experimental results led to the characterisation of three different flow

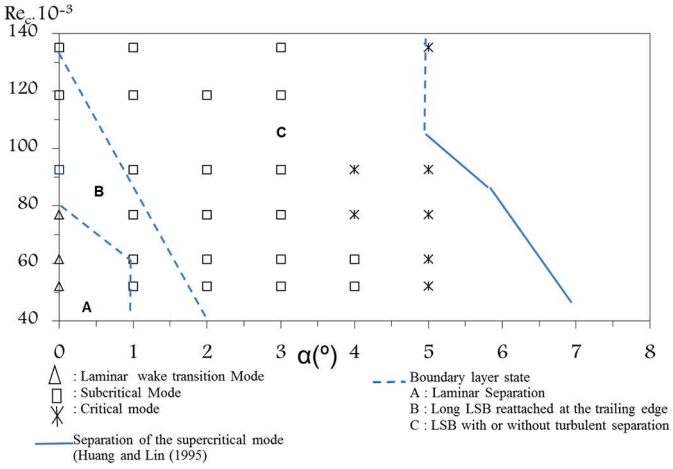

Fig. 7. Flow regimes in the wake and boundary layer state expressed in terms of chord Reynolds number and angle of attack.

regimes as shown in Figure 7. This figure summarizes these results and compares them to Huang and Lin's [18] results. A laminar regime with laminar Kármán streets is obtained for low angles of attack and Reynolds numbers. This regime correspond to the laminar mode A' of Huang and Lin [18]. The subcritical mode with a turbulent Kármán vortex streets seems to extend more in our case than the B′ of Huang and Lin [18]; a critical transition regime with non-structured Kármán vortex streets follows. The differences observed are essentially due to the geometric difference. In fact, the cantilever airfoil analysed in Huang and Lee [19] work is more subject to 3D effects than what we experienced in our setup.

4 Discussion

In this discussion, we represent in Figure 7 the boundary layer state along with the different regimes describing the wake dynamics, as the angle of attack and Reynolds number increased. In particular, we observed the following.

1. A laminar regime with laminar Kármán streets, while the boundary layer is laminar with a laminar separation ($52\,000 < \mathrm{Re}_c < 61\,400$, $\alpha = 0°$).
2. A subcritical transitional regime with a turbulent Kármán vortex streets, along with a very long laminar separation bubble with a turbulent reattachment very close to the trailing edge ($52\,000 < \mathrm{Re}_c < 61\,400$, $\alpha = 1°$ or $77\,000 < \mathrm{Re}_c < 1\,18\,600$, $\alpha = 0°$).
3. A critical transition regime with non-structured Kármán vortex streets, associated with an LSB followed by a turbulent boundary layer ($52\,000 < \mathrm{Re}_c < 61\,400$, $\alpha = 2\,°$, or $77\,000 < \mathrm{Re}_c < 1\,18\,600$, $\alpha = 1°$, or $\mathrm{Re}_c = 1\,35\,200$, $\alpha = 0°$).

From Figure 7, we observe the region below $\mathrm{Re}_c = 90 \times 10^3$ corresponding to the region where the maximum amplitude stayed constant with air speed in the

pitching airfoil experiment. A separation for a small zone A at low angle of attack below $\alpha = 1°$ is followed by LSB appearance. Its size experienced reduction with increasing angle of attack. We can expect to see this evolution of the boundary layer during a pitching cycle for the oscillating airfoil. During such cycle, the wake goes through the three modes while the angle of attack changes from zero to the maximum angle of 5°. Above the $\mathrm{Re}_c = 90 \times 10^3$ line, corresponds to the region where the maximum amplitude decreased with speed for the pitching airfoil. It ends at $\alpha = 3°$. A LSB is always present but becomes shorter with the increasing angle of attack. This region is characterised by a wake in a subcritical mode. The reduction of the size of the LSB leads to its cycle period reduction, this is in line with the increase in the pitching frequency reported in [10].

5 Conclusions

This study has documented the flow structure and modes over the boundary layer and the wake of a NACA0012 airfoil in static conditions at transitional chord-based Reynolds numbers, for small angles of attack. A laminar mode, with a laminar separation on the boundary layer and laminar Kármán streets in the wake, is first observed for $\mathrm{Re}_c < 61\,400$ and $\alpha = 0°$. At $77\,000 < \mathrm{Re}_c < 1\,18\,600$, corresponding to a subcritical mode, the boundary layer presents a long separation bubble reattached close to the trailing edge, and the wake shows turbulent Kármán streets. Finally, for higher Re_c and α, a critical transition mode consists of a long bubble followed by a turbulent boundary layer, and less-structured Kármán street in the wake of the airfoil. The flow characteristics observed are generally similar to those highlighted by previous authors, but some considerable differences in the flow separation localisation at the airfoil surface have been noticed from measurements performed with different techniques, namely oil-flow visualizations and hot-film measurements.

Nomenclature

C	Airfoil chord length
f	Frequency
k	Reduced frequency $= fC/2U$
Re_c	Chord-based Reynolds number
St	Stouhal number $= fC/U$
U	Free stream velocity
u'	Streamwise velocity fluctuation
v'	Transverse velocity fluctuation
X	Chordwise coordinate
α	Angle of attack
$\phi_{\beta\beta}$	Power spectrum of β (u'or v')
CTA	Constant Temperature Anemometry
DNS	Direct Numerical Simulation
LES	Large Eddy Simulation
LSB	Laminar Separation Bubble
LCO	Limit Cycle Oscillations

The financial support of the Department of National Defence Canada (DND), through the CDARP and of the Natural Sciences and Engineering Research Council of Canada (NSERC) are gratefully acknowledged.

References

[1] T. Kinsey, G. Dumas, G. Lalande, J. Ruel, A. Mehut, P. Viarouge, J. Lemay, Y. Jean, Prototype testing of a hydrokinetic turbine based on oscillating hydrofoils. Renew. Energy **36**, 1710–1718 (2011)

[2] M. Gaster, The structure and behaviour of laminar separation bubbles. Aeronautical Research Council Reports and Memoranda-Report No 3595 (1967)

[3] O. Marxen, D.S. Henningson, The effect of small-amplitude convective disturbances on the size and bursting of a laminar separation bubble. J. Fluid Mech. **671**, 1–33 (2011)

[4] A. Roshko, On the development of turbulent wakes from vortex streets. Tech. rep., National Advisory Committee for Aeronautics. Tech Note 2913. California Institute of Technology (1954)

[5] C.H. Williamson, Vortex dynamics in the wake of a cylinder. In *Fluid vortices*. Springer (1995) 155–234

[6] B. Carmichael, Low reynolds number airfoil survey, volume 1. Tech. rep., NASA, contrator Report 165803 (1981)

[7] P. Lissaman, Low-reynolds-number airfoils. Annu. Rev. Fluid Mech. **15**, 223–239 (1983)

[8] P. Balakumar, Direct numerical simulation of flows over an naca-0012 airfoil at low and moderate reynolds numbers. In 47th AIAA Fluid Dynamics Conference (2017), p. 3978

[9] L.B. Streher, Large-eddy simulation of the flow around a naca-0012 airfoil at different amgles of attack. Master's thesis, Helmut Schmidt University, 2017

[10] D. Poirel, Y. Harris, A. Benaissa, Self-sustained aeroelastic oscillations of a naca0012 airfoil at low-to-moderate Reynolds numbers. J. Fluids Struct. **24**, 700–719 (2008)

[11] C.J. Barnes, M.R. Visbal, On the role of flow transition in laminar separation flutter. J. Fluids Struct. **77**, 213–230 (2018)

[12] A. Poels, D. Rudmin, A. Benaissa, D. Poirel, Localization of flow separation and transition over a pitching naca0012 airfoil at transitional reynolds numbers using hot-films. J. Fluids Eng. **137**, 124501 (2015)

[13] D. Poirel, Y. Harris, A. Benaissa, Aeroelastic dynamics of a naca 0012 airfoil in the transitional reynolds number regime. In ASME 2006 Pressure Vessels and Piping/ICPVT-11 Conference, American Society of Mechanical Engineers (2006) 847–854

[14] B. McGranahan, M. Selig, Surface oil flow measurements on several airfoils at low Reynolds numbers. In 21st AIAA Applied Aerodynamics Conference (2003) 4067

[15] D. Rudmin, Detection of laminar flow separation and transition on a piching naca0012 airfoil. Master's thesis, Mechanical and Aerospace Engineering, Royal Military College of Canada (2012)

[16] D. Rudmin, A. Benaissa, D. Poirel, Detection of laminar flow separation and transition on a naca-0012 airfoil using surface hot-films. J. Fluids Eng. **135**, 101104 (2013)

[17] H.-W. Lee, R.-F. Huang, Frequency selection of wake flow behind a naca 0012 wing. J. Mar. Sci. Technol. **6**, 29–37 (1998)

[18] R.F. Huang, C.L. Lin, Vortex shedding and shear-layer instability of wing at low-Reynolds numbers. AIAA J. **33**, 1398–1403 (1995)

[19] R.F. Huang, H.W. Lee, Effects of freestream turbulence on wing-surface flow and aerodynamic performance. J. Aircraft **36**, 965–972 (1999)

[20] Y. Jung, S.O. Park, Vortex-shedding characteristics in the wake of an oscillating airfoil at low reynolds number. J. Fluids Struct. **20**, 451–464 (2005)

Cite this article as: A. Poels, X. Collin, A. Benaissa, D. Poirel, Mode and regime identification for a static NACA0012 airfoil at transitional Reynolds numbers, Mechanics & Industry **21**, 620 (2020)